POTENTIAL CLINICAL RELEVANCE

Nanomedicine: Nanotechnology, Biology, and Medicine
8 (2012) 228–236

Research Article

nanomedjournal.com

In vivo cancer imaging by poly(ethylene glycol)-*b*-poly(ε-caprolactone) micelles containing a near-infrared probe

Hyunah Cho, MS[a], Guilherme L. Indig, PhD[c], Jamey Weichert, PhD[d], Ho-Chul Shin, MS[a], Glen S. Kwon, PhD[a,b,*]

[a]*Department of Pharmaceutical Science, School of Pharmacy, University of Wisconsin, Madison, Wisconsin, USA*
[b]*College of Pharmacy, Kyung Hee University, Seoul, South Korea*
[c]*Department of Chemistry and Biochemistry, University of Wisconsin, Milwaukee, Wisconsin, USA*
[d]*Department of Radiology, School of Medicine and Public Health, University of Wisconsin, Madison, Wisconsin, USA*

Received 10 November 2010; accepted 8 June 2011

Abstract

Noninvasive near-infrared (NIR) fluorescence imaging is a promising technique for the intraoperative assessment of solid tumor removal. We incorporated a lipophilic NIR probe, 1,1′-dioctadecyltetramethyl indotricarbocyanine iodide (DiR), in poly(ethylene glycol)-*b*-poly(ε-caprolactone) (PEG-*b*-PCL) micelles, resulting in DiR solubilization in water, occupying nanoscopic PEG-*b*-PCL micelles. DiR in a self-quenched or nonquenched state showed different kinetics of release from PEG-*b*-PCL micelles in vitro; however, both obtained high tumor delineation (tumor-to-muscle ratio of 30–43 from collected organs). These results suggest that PEG-*b*-PCL micelles with DiR are a promising nanosized imaging agent that will provide a basis for enhanced surgical guidance via NIR visualization of tumors.

From the Clinical Editor: In this paper, noninvasive near-infrared fluorescence imaging coupled with specific lipophilic probes is discussed as a promising technique for intraoperative assessment of solid tumor removal, leading to optimized outcomes for in toto removal of tumors.

Key words: Near infrared (NIR) fluorescence imaging; Poly(ethylene glycol)-*b*-poly(ε-caprolactone); Polymeric micelles; Self-quenching

In a clinical point of view, NIR probe-incorporated polymeric micelles could be used for both the diagnosis of tumors and the guidance of surgery. Surgical removal of tumors is the best method to treat cancers if the entire tumor can be completely removed. However, complete tumor removal depends on how well the tumor is delineated and how impeccably surgery is performed.[1-13] Monitoring the presence of tumor tissues remaining in surrounding surgical margins by using NIR probe-incorporated polymeric micelles and the removal of tumor tissues are prudent courses of action for avoiding recurrence.[14] It is expected that NIR probe-incorporated polymeric micelles can provide decisive guidance for improved surgical removal of tumors. In this study, we investigated the optical imaging of cancer by NIR probe-incorporated polymeric micelles in a xenograft model. DiR is a lipophilic carbocyanine dye that is strongly light-absorbing and used as a tool in different research areas, such as lipid membrane-potential sensor, organelle stains for mitochondria and endoplasmic reticulum and long-term labeling of cells in culture.[15,16] For optical imaging, DiR absorbs in the NIR region (λ_{max} = 750 nm), and it has a high quantum yield. For the clinical applications in optical imaging, PEG-*b*-PCL micelles are a promising class of nanocarriers for DiR for the following reasons: The preparation of PEG-*b*-PCL micelles that contain DiR is facile; PEG-*b*-PCL micelles increase the water solubility of the highly lipophilic DiR in aqueous solution;[17-22] PEG-*b*-PCL micelles have prolonged in vivo circulation due to the kinetic stability of PEG-*b*-PCL micelles in blood with respect to disassembly and the avoidance of the reticuloendothelial system by PEG-*b*-PCL micelles.[23] As a result, passive tumor targeting of PEG-*b*-PCL micelles has been achieved by the EPR effect[20,23] in xenograft models. We studied PEG-*b*-PCL micelles with NIR probe, DiR, in a quenched or nonquenched state. Although both states showed different kinetic profiles for NIR probe release in vitro and photophysical properties in vivo, both states achieved high signals in tumor tissues for optical imaging.

The authors report no conflicts of interest.

*Corresponding author: Department of Pharmaceutical Science, School of PharmacyUniversity of Wisconsin, Madison, WI 53705, USA.
E-mail address: GSKwon@Pharmacy.wisc.edu (G.S. Kwon).

1549-9634/$ – see front matter © 2012 Elsevier Inc. All rights reserved.
doi:10.1016/j.nano.2011.06.009

Please cite this article as: H. Cho, G.L. Indig, J. Weichert, H.-C. Shin, G.S. Kwon, In vivo cancer imaging by poly(ethylene glycol)-*b*-poly(ε-caprolactone) micelles containing a near-infrared probe. *Nanomedicine: NBM* 2012;8:228-236, doi:10.1016/j.nano.2011.06.009

Methods

Preparation and characterization of PEG-b-PCL micelles with DiR

DiR-loaded PEG-*b*-PCL micelles were prepared by dissolving 4.0–200 mg of PEG-*b*-PCL (5k:10k, Mw/Mn: 1.3),(Polymer Source, Dorval, Quebec, Canada) and 0.10–0.50 mg of DiR (Invitrogen, Carlsbad, California) in acetone (2.0 mL) followed by the dropwise addition of 0.9% sodium chloride (2.0 mL) by a syringe at a flow rate of 1.0 mL sec^{-1} with vigorous mixing. Acetone was evaporated from the aqueous solution by stirring at room temperature (20–25°C) for 1 hour. The PEG-*b*-PCL solution was centrifuged for 5 minutes at 10,000*g* to remove unincorporated DiR that was insoluble. The aqueous micelle solution was filtered through 0.45 μm nylon syringe filter (National Scientific, Rockwood, Tennessee). The aqueous solubility of DiR was determined by UV-visible measurements on a Cary 100 Bio UV-visible spectrophotometer (Varian, Palo Alto, California). Particle-size distributions of PEG-*b*-PCL micelles with DiR were determined by dynamic light scattering (DLS) measurement, using a Zetasizer Nano-ZS (Malvern Instruments, Ltd., Malvern, United Kingdom) at a detection angle of 173 degrees and a He–Ne ion laser (λ = 633 nm) for the incident beam. Fluorescence measurements on DiR were conducted on AMINCO-Bowman Series 2 spectrofluorometer (Thermo Scientific, Rockford, Illinois) with excitation and emission wavelengths at 745 and 800 nm, respectively. For fluorescence measurements on DiR, absorbances were kept below 0.3 to preclude inner filter effects. The fluorescence self-quenching of DiR as a function of its loading in PEG-*b*-PCL micelles was evaluated by monitoring its fluorescence emission relative to its fluorescence emission upon 100% DiR release from PEG-*b*-PCL micelles; this was realized by freeze-drying of an aliquot of PEG-*b*-PCL micelles, followed by dissolution of the solid sample in acetone and measurement of DiR fluorescence.

In vitro DiR release profile for PEG-b-PCL micelles

Aqueous micelle solutions (2.5 mL) were loaded into 20,000 MWCO Slide-A-Lyser dialysis cassettes (Thermo Scientific) and cassettes (n = 4) were then placed in 0.9% sodium chloride solution (2.0 L) at 37°C with stirring. The sodium chloride solution was refreshed every 3 hours to ensure sink conditions. Samples of 100 μL were withdrawn from cassettes, and cassettes were replenished with 100 μL fresh sodium chloride solution. Sampling intervals were 1, 2, 3, 6, 12, 24, 48, 72 and 96 hours. Withdrawn samples at each time point were analyzed for the amount of DiR release on a Cary 100 Bio UV-visible spectrophotometer (Varian).

Xenograft model

LS180 human colon carcinoma cells (kindly provided by Dr. Jamey Weichert, University of Wisconsin-Madison) were cultivated in minimum essential medium including Earle's salts (Cellgro, Manassas, Virginia), supplemented with 2% sodium bicarbonate, 1% nonessential amino acids, 1% sodium pyruvate, 10% fetal bovine serum, 1% L-glutamine and 100 U mL^{-1} penicillin-streptomycin solution. Cultivated cells were kept at 37°C under an atmosphere of 5% CO_2 in a humidified incubator. About 1 week prior to imaging, 1×10^6 LS180 cells were inoculated subcutaneously into the right flanks of anesthetized female 6- to 8-week-old athymic nude mice (Laboratory Animal Resources, Madison, Wisconsin). General anesthesia was induced with 1.5% isoflurane/oxygen and anesthesia was maintained with 1% isoflurane/oxygen. All animal experiments were performed with human care of animals and approved by University of Wisconsin-Madison's Institutional Animal Care and Use Committee guidelines, and procedures were in accordance with the institutional guidance.

Animal surgery and tissue excision

Animals were treated in a sterile environment. Ninety-six hours after injection of PEG-*b*-PCL micelles with DiR, mice were sacrificed by CO_2 asphyxia. A midline incision was done with microsurgical instruments under white light illumination, and organs such as liver, lung, heart, spleen, and kidneys, as well as muscle tissue, were removed. The skin of mice was also removed over the tumor and tumor excision was performed.

NIR fluorescence imaging of DiR

For imaging, DiR-loaded PEG-*b*-PCL micelles, representing 10 μg of DiR, were injected in the tail vein of anesthetized animals when sizes of tumors reached to 80–100 mm^3. Whole-body fluorescence images were recorded 10 minutes, 1, 4, 9, 12, 24, 48, 72 and 96 hours after intravenous administration using Xenogen IVIS 200 Series (Caliper Life Sciences, Hopkinton, Massachusetts) equipped with a 150-watt quartz halogen lamp and a 1-mW power scanning laser. Mice (n = 3 for each micelle formulation) were placed in the dorsal and lateral positions to obtain whole-body optical images. Tumors, organs and tissues removed at 96 hours post injection were scanned before dehydration began and their ex vivo images were obtained. All images were acquired by back-thinned, back-illuminated grade 1 CCD camera with the following parameters: exposure time = 1 second; binning = medium; f/stop 2. Filter sets were fixed with the following parameters for DiR: excitation at 745 nm and emission at 800 nm. Acquired images were measured and analyzed with Living Imaging software (Caliper Life Sciences). The distribution of DiR in the whole body was quantified by average radiant efficiency, total photons per second per square centimeter per steradian in the irradiance range (microwatts per square centimeter): [p s^{-1} cm^{-2} sr^{-1}]/[μW cm^{-2}]. The tumor-specific accumulation of DiR was evaluated by signal-to-noise ratio: average radiant efficiency at the region of interest (ROI) was drawn around the tumor to average radiant efficiency at the opposite region indicating background tissue (left flank). Horizontal radiant efficiency maps were drawn by Living Imaging software according to the fluorescence intensity of DiR at the horizontal line passing through the center of a tumor. DiR uptake values in organs and tumors were calculated by its fluorescence relative to its

Table 1
Z-average diameters of DiR-loaded PEG-*b*-PCL micelles and aqueous solubility of DiR

Micelles (DiR:PEG-b-PCL) (weight:weight)	Z-average diameter (nm)	PDI	Aqueous solubility of DiR in micelle formulations (μg/mL)
1:40 (Self-quenching)	47.06 ± 1.80	0.154 ± 0.017	44.52 ± 4.05
1:25	41.9 8 ± 0.44	0.123 ± 0.014	56.37 ± 8.01
1:33	41.76 ± 3.39	0.088 ± 0.065	137.9 ± 5.49
1:50	37.80 ± 0.88	0.044 ± 0.035	150.5 ± 6.33
1:80	36.61 ± 0.75	0.062 ± 0.029	175.7 ± 2.98
1:100	32.29 ± 3.46	0.055 ± 0.024	176.9 ± 4.15
1:400 (Non-quenching)	31.90 ± 1.07	0.044 ± 0.054	229.9 ± 3.07

Data are expressed as mean ± SD (n = 3). ∗PDI (polydispersity index).

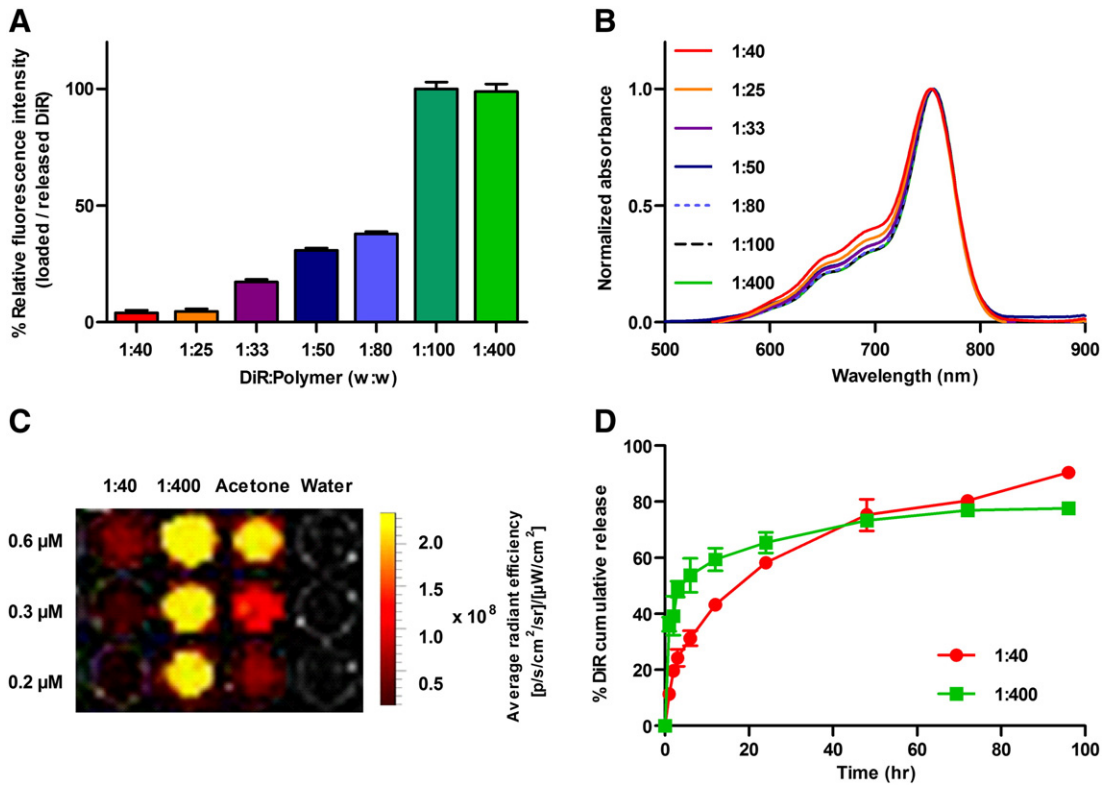

Figure 1. **(A)** Fluorescence intensity of DiR-loaded PEG-*b*-PCL micelles relative to free DiR, and **(B)** Normalized absorbance spectra of DiR-loaded PEG-*b*-PCL micelles at varied ratios of DiR to PEG-*b*-PCL. **(C)** Fluorescence images of DiR (0.6, 0.3 and 0.2 μM) in a multi-well format obtained by Xenogen IVIS 200 Series; DiR-loaded PEG-*b*-PCL micelles (1:40 and 1:400), DiR in acetone, and water (autofluorescence). **(D)** In vitro release profiles of DiR from PEG-*b*-PCL micelles (1:40 and 1:400).

fluorescence in muscles after tissue excision. In vitro fluorescence measurements of DiR-loaded PEG-*b*-PCL micelles seeded in 96-well black fluorescence microplates were also performed using the Xenogen IVIS200 Series.

Results

Characterization of DiR-loaded PEG-b-PCL micelles

Table 1 shows the results on the solubilization of DiR by PEG-*b*-PCL micelles at varied ratios of DiR to PEG-*b*-PCL. DiR is practically insoluble in water (< 1.0 μg/mL). PEG-*b*-PCL micelles readily increased the water solubility of DiR from 44 to 230 μg/mL with an increase in the quantity of PEG-*b*-PCL. The loading efficiency (wgt $DiR_{PEG\text{-}b\text{-}PCL}$ /wgt $DiR_{initial}$) was approximately 90%. At a low DiR-to-PEG-*b*-PCL ratio (1:400), PEG-*b*-PCL micelles had an average hydrodynamic diameter of 32 nm with a low polydispersity index (PDI). At a higher ratio of DiR to PEG-*b*-PCL (1:40), PEG-*b*-PCL micelles had a higher average hydrodynamic diameter of 47 nm and higher PDI, possibly due to a higher average number of DiR per micelle. Assuming that the association number of PEG-*b*-PCL micelles is 200,[19] there were about 7 DiR per PEG-*b*-PCL micelle at the DiR-to-PEG-*b*-PCL ratio of 1:400, whereas there were about 74 DiR per PEG-*b*-PCL micelle at the DiR-to-PEG-*b*-PCL ratio of 1:40.

Self-quenching of DiR in PEG-b-PCL micelles

Figure 1, *A* shows the relative fluorescence intensity of DiR at varied ratios of DiR to PEG-*b*-PCL. At a ratio of 1:400, the fluorescence of DiR incorporated in PEG-*b*-PCL micelles was close to the fluorescence of DiR after 100% release from PEG-*b*-PCL micelles in acetone, suggesting that DiR in the core region exists in a non-self-quenched state (monomers). As the content of DiR increased in PEG-*b*-PCL micelles, there was a loss in quantum yield, presumably due to DiR-self-quenching at higher levels of multiply occupied PEG-*b*-PCL micelles. At a ratio of 1:40, the fluorescence of DiR incorporated in PEG-*b*-PCL micelles was less than 10% relative to the acetone control. At about 74 DiR per PEG-*b*-PCL micelle, DiR self-quenching is evident, consistent with multiply occupied PEG-*b*-PCL micelles that have cores with diameters less than 10 nm and the presence of ground-state species of DiR. The absorption spectra of DiR at varied ratios of DiR to PEG-*b*-PCL are consistent with DiR self-quenching in PEG-*b*-PCL micelles at high loading (Figure 1, *B*). As the ratio increased, absorption bands at lower wavelengths relative to the major absorption band of DiR at 745 nm increased. The absorption bands at 650 and 692 nm signify the self-association of DiR in PEG-*b*-PCL micelles, resulting in the self-quenching of fluorescence. The in vitro fluorescence intensity of DiR detected by IVIS 200 Series in a 96-well plate is shown in Figure 1, *C*. At a ratio of 1:400, the fluorescence of DiR loaded in PEG-*b*-PCL micelles showed the highest intensity, whereas at a ratio of 1:40, the fluorescence of DiR loaded in PEG-*b*-PCL micelles had a lower intensity than DiR solubilized in acetone at the same level. The fluorescence intensities of DiR in PEG-*b*-PCL micelles and acetone were concentration dependent. In summary, PEG-*b*-PCL micelles could effectively raise the water solubility of DiR and DiR existed in either a quenched or nonquenched state in the cores of PEG-*b*-PCL micelles, depending on the extent of DiR incorporation.

In vitro DiR release kinetics for PEG-b-PCL micelles

The release kinetics of DiR for PEG-*b*-PCL micelles at 1:40 (self-quenched) and 1:400 (nonquenched) ratios were investigated (Figure 1, *D*). At a 1:40 ratio, DiR was gradually released from PEG-*b*-PCL micelles with the half-life for DiR release at approximately 20 hours. On the other hand, the release of DiR from PEG-*b*-PCL micelles at a ratio of 1:400 was biphasic, and most of the DiR was released from PEG-*b*-PCL micelles over 6 hours, followed by a more gradual release profile over 24 hours. The half-life for nonquenched DiR release was approximately 1 hour. After 48 hours, 70% of the DiR had been released from PEG-*b*-PCL micelles irrespective of the quenched state of the DiR. It is assumed that self-quenched DiR molecules in PEG-*b*-PCL micelles at a 1:40 ratio are aggregated and slowly transform into monomers as function of time. This release profile for DiR from PEG-*b*-PCL micelles was further verified with in vivo optical imaging experiments.

NIR fluorescence imaging of DiR-loaded PEG-b-PCL micelles in tumor-bearing mice

Tumor-specific accumulation of PEG-*b*-PCL micelles that contain DiR was determined using noninvasive optical imaging based on fluorescence intensity of DiR. The time-dependant whole-body biodistribution of PEG-*b*-PCL micelles that have quenched or nonquenched DiR was monitored by radiant efficiency (Figures 2, *A* and 2, *B*). In a quenched state (1:40), the fluorescence of DiR gradually emerged from the dorsal and lateral portions of the mice over several hours (Figure 2, *E*). On the other hand, DiR in a nonquenched state (1:400) showed a rapid onset of fluorescence intensity that was much stronger than that of DiR in a quenched state. Although the fluorescence signal of DiR slowly decreased after approximately 10 minutes, the fluorescence signal of quenched DiR increased over time, reaching a similar value at dorsal and lateral sites after approximately 24–48 hours. Figures 2, *C* and 2, *D* show the fluorescence intensity of DiR following a horizontal line passing through tumors. Radiant-efficiency maps of DiR taken at various time points after injection of the PEG-*b*-PCL micelles that contain quenched DiR showed gradual tumor-specific accumulation of DiR as function of time; the strongest signal from the tumor region was observed after 12 hours and the lowest signal from DiR was detected at 10 minutes post injection. On the other hand, maps for PEG-*b*-PCL micelles that contain nonquenched DiR showed an opposite tendency; the strongest fluorescence signal of DiR was observed within 1 hour after injection, whereas the lowest signal of DiR was obtained after 72 hours. Tumor-to-muscle ratios for DiR indicate that the tumor-specific accumulation efficiencies were not significantly different for the quenched and nonquenched groups. The ratios were calculated to be approximately 2; however, the ratios calculated from 1:40 group were slightly higher than the ratios for the 1:400 group (Figure 2, *F*). The DiR solubilized in 20% DMSO solution was also injected into xenograft mice through the tail vein but no tumor specific accumulation could be observed. Moreover, the whole-body signal was so weak that the biodistribution of DiR could not be visualized with the same fluorescence intensity scale that was used for PEG-*b*-PCL micelles (see Supplementary Material). These results suggest that DiR-incorporated PEG-*b*-PCL micelles are superior to free DiR for visualizing tumor tissues in living mice. No notable toxicity of DiR-loaded PEG-*b*-PCL micelles during the animal experiments was found.

Ex vivo NIR fluorescence imaging of DiR-loaded PEG-b-PCL micelles in excised tissues

Color-coded NIR fluorescence images of excised tissues (lung, heart, spleen, tumor, kidneys, liver and muscle) (Figures 3, *A* and 3, *B*) were obtained after 96 hours. Fluorescence images showed that the strongest signal of DiR was observed in tumor tissues, followed by the liver and spleen, for both quenched and nonquenched groups of DiR-loaded PEG-*b*-PCL micelles. The optical signal of DiR from the lungs was also relatively strong for PEG-*b*-PCL micelles with nonquenched DiR (Figure 3, *B*). The fluorescence intensity ratio of tumor to muscle was approximately 30 for PEG-*b*-PCL micelles with quenched DiR, whereas the fluorescence intensity ratio of tumor to muscle was approximately 43 for PEG-*b*-PCL micelles with nonquenched DiR (Figure 3, *C*).

Residual tumor detection after surgical removal

Xenograft animals were sacrificed 96 hours post injection and their dorsum was opened, guided by the strong fluorescence signal of DiR. Tumor tissue was selectively visualized in the

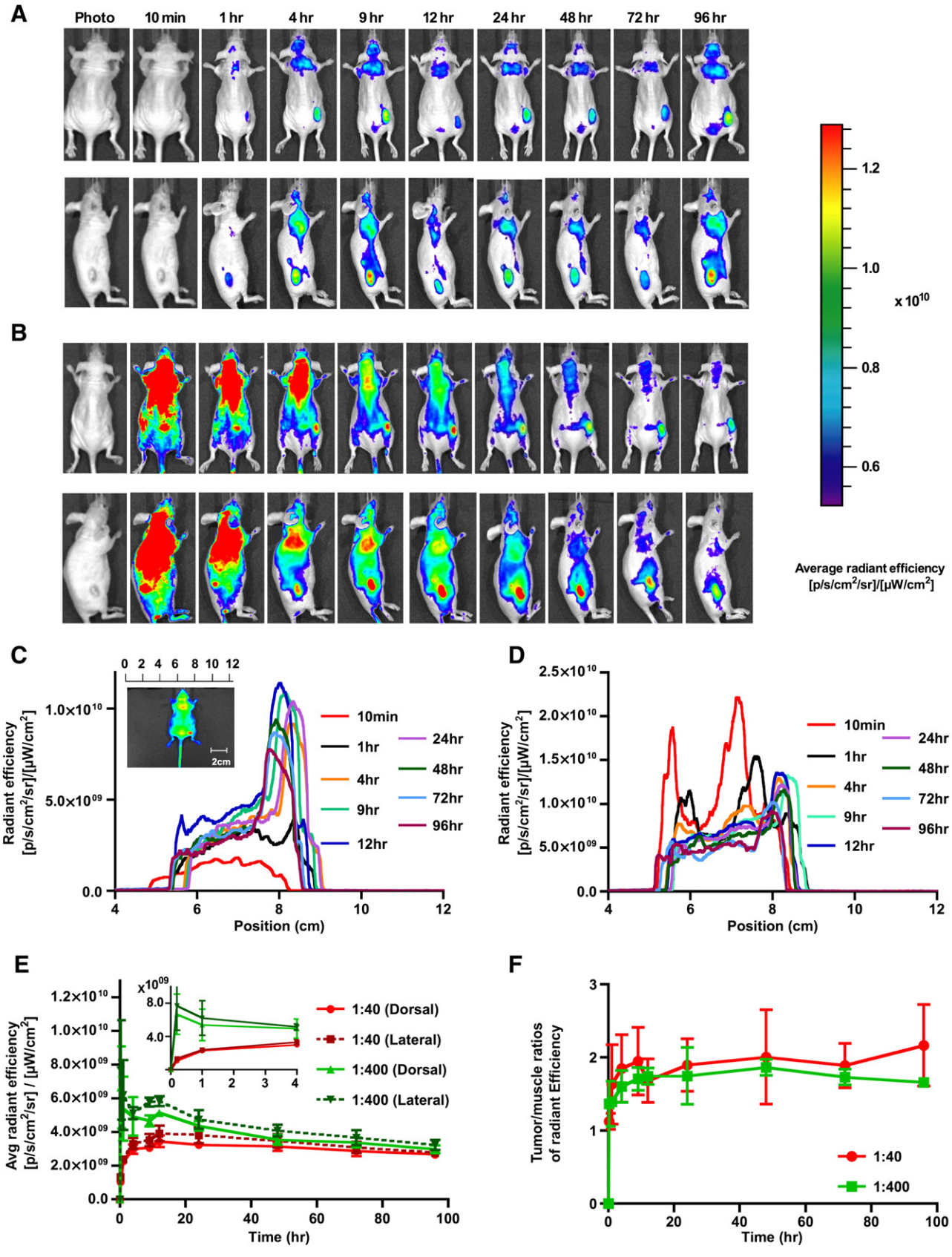
A
Photo
10 min
1 hr
4 hr
9 hr
12 hr
24 hr
48 hr
72 hr
96 hr
B
1.2
1.0
0.8
0.6
x 10^10
Average radiant efficiency [p/s/cm²/sr]/[μW/cm²]
C
Radiant efficiency [p/s/cm²/sr]/[μW/cm²]
1.0x10^10
5.0x10^09
0.0
0 2 4 6 8 10 12
2cm
10min
1hr
4hr
9hr
12hr
24hr
48hr
72hr
96hr
4 6 8 10 12
Position (cm)
D
Radiant efficiency [p/s/cm²/sr]/[μW/cm²]
2.5x10^10
2.0x10^10
1.5x10^10
1.0x10^10
5.0x10^09
0.0
10min
1hr
4hr
9hr
12hr
24hr
48hr
72hr
96hr
4 6 8 10 12
Position (cm)
E
Avg radiant efficiency [p/s/cm²/sr] / [μW/cm²]
1.2x10^10
1.0x10^10
8.0x10^09
6.0x10^09
4.0x10^09
2.0x10^09
0.0
x10^09
8.0
4.0
0 1 2 3 4
1:40 (Dorsal)
1:40 (Lateral)
1:400 (Dorsal)
1:400 (Lateral)
0 20 40 60 80 100
Time (hr)
F
Tumor/muscle ratios of radiant Efficiency
3
2
1
0
1:40
1:400
0 20 40 60 80 100
Time (hr)

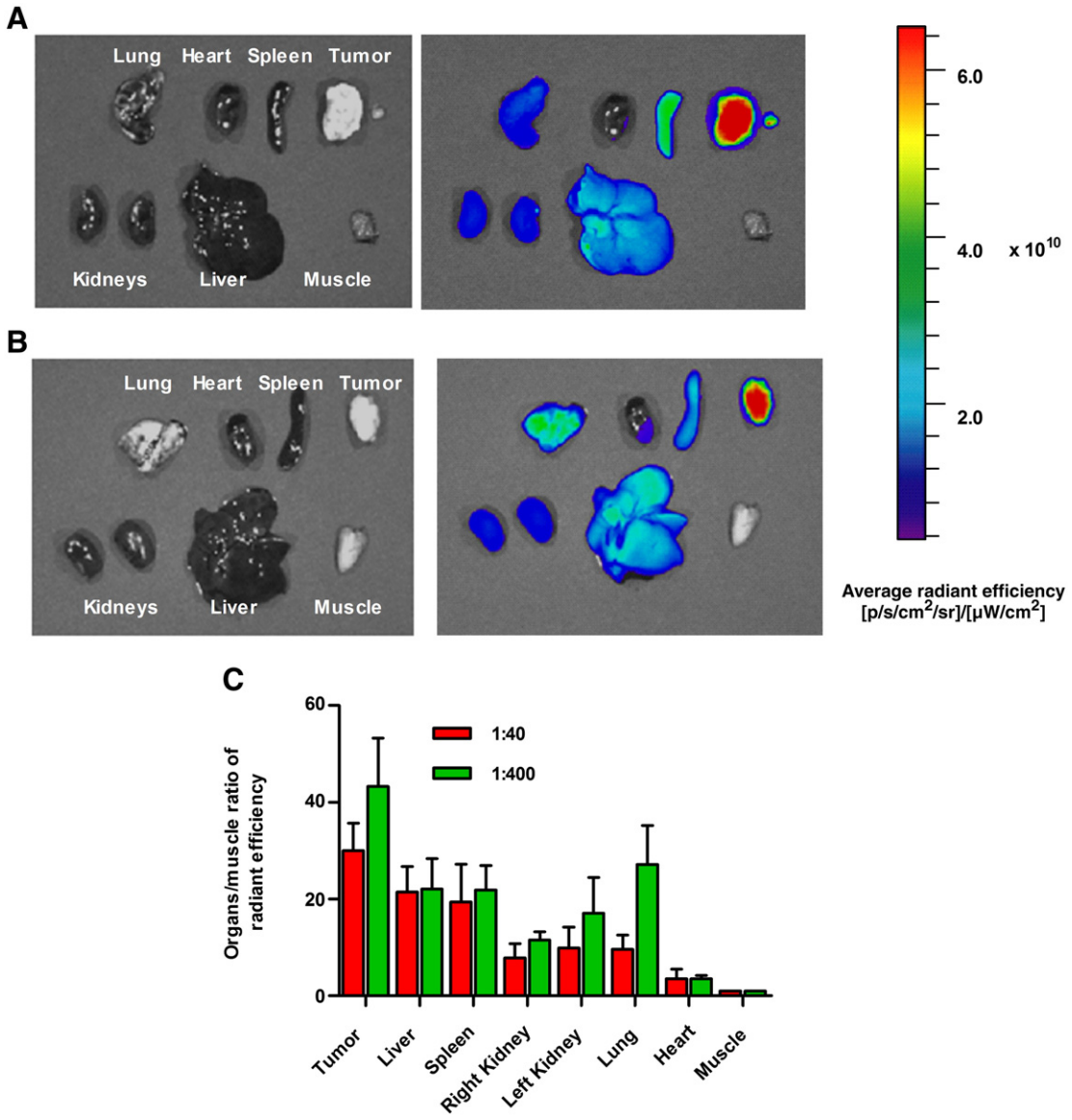

Figure 3. Ex vivo optical images of tissues for **(A)** DiR-loaded PEG-*b*-PCL micelles (1:40) and **(B)** DiR-loaded PEG-*b*-PCL micelles (1:400). **(C)** Relative radiant efficiency of DiR distributed in excised organs in comparison with muscle after 96 hrs.

incised animal body due to NIR fluorescence emitted by DiR-loaded PEG-*b*-PCL micelles (Figure 4, *A*).

The completeness of tumor removal depends on how finely the tumor is delineated before and during surgery. The LS180 human colon carcinoma solid tumor was removed as completely as possible from the xenograft animal under white light and residual tumor was detected by NIR fluorescence imaging of DiR (Figure 4, *B*). A weak fluorescence signal from DiR was detectable at the site of tumor resection, pointing to remaining tumor margins that were not clearly observable by the naked eye during the surgical removal of the primary tumor (Figure 4, *C*).

Discussion

In this study, DiR was successfully incorporated into PEG-*b*-PCL micelle by a simple nano-precipitation method and the average diameter of DiR-loaded PEG-*b*-PCL micelles was about

Figure 2. Real time in vivo fluorescence whole-body images of mice with LS180 human colon carcinoma xenografts. Time-dependent images of **(A)** DiR-loaded PEG-*b*-PCL micelles (1:40) **(B)** DiR-loaded PEG-*b*-PCL micelles (1:400) in dorsal (upper) and lateral (below) views. Time-dependent radiant efficiency maps according to horizontal lines passing through the center of tumors for **(C)** DiR-loaded PEG-*b*-PCL micelles (1:40) and **(D)** DiR-loaded PEG-*b*-PCL micelles (1:400). **(E)** Calculated average radiant efficiency of DiR-loaded PEG-*b*-PCL micelles (1:40 and 1:400) in dorsal portions and lateral views as a function of the time based on Figures 2, *A* and *B* (Expanded figure from 0 to 4 hr time point was inserted). **(F)** Relative radiant efficiency of DiR distributed in tumors in comparison with muscles over time in living mice.

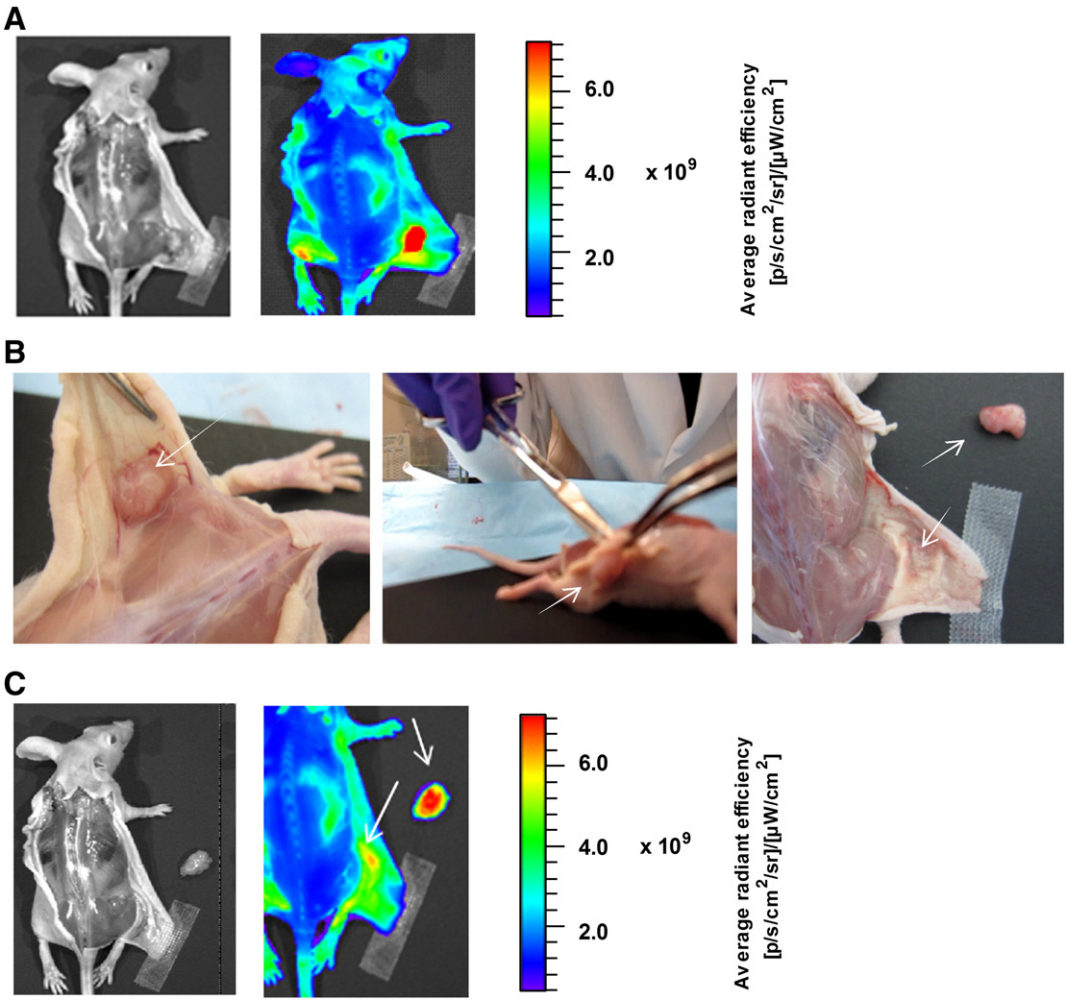

Figure 4. Detection of tumor and margins before and after surgery by DiR-loaded PEG-*b*-PCL micelles (1:400). **(A)** Before surgery, **(B)** surgical tumor removal and **(C)** after surgery.

30–50 nm. PEG-*b*-PCL micelles substantially increased the water solubility of DiR, enabling optical imaging experiments in mice. As shown in Table 1, the content of DiR in PEG-*b*-PCL micelles could be controlled, resulting in PEG-*b*-PCL micelles that are multiply occupied by DiR. At low occupancy (1:400), photophysical experiments on DiR suggest that the dye exists in a nonquenched state in the cores of PEG-*b*-PCL micelles. At high occupancy (1:40), DiR exists in a quenched state in the cores of PEG-*b*-PCL micelles, probably due to the existence of ground-state species of DiR. Carbocyanine dyes tend to self-associate and exist as H-aggregates. H-aggregates are a one-dimensional array of dyes in which the transition moments of individual monomers are aligned parallel to each other, but perpendicular to the line joining their centers (face-to-face arrangement).[24-28] H-aggregates of DiR do not emit typical fluorescence and their excited states are rapidly deactivated by internal conversion and intersystem crossing. H-aggregates show lower fluorescence intensity than monomers and display blue-shifted absorption spectrum (Figures 1, *A* and 1, *B*).[29,30] At a ratio of 1:40, DiR molecules are positioned closely and exist also as H-aggregates in the cores of PEG-*b*-PCL micelles, whereas at a ratio of 1:400, DiR molecules are widely separated and exist predominantly as monomers in the cores of PEG-*b*-PCL micelles, resulting in a strong fluorescence signal in comparison with DiR in acetone (Figure 1, *C*).

Most researchers have endeavored to avoid dye aggregation and the loss of fluorescence quantum yield for optical imaging.[9] However, we noticed differences in the in vitro kinetics of DiR release for PEG-*b*-PCL micelles, depending on the quantity of incorporated DiR (1:40 versus 1:400) and speculated that in vivo optical imaging of DiR in a xenograft model would depend on the release kinetics of DiR from PEG-*b*-PCL micelles. Presumably, H-aggregates of DiR in the cores of PEG-*b*-PCL micelles at 1:40 ratio are responsible for the slow release pattern of DiR obtained in vitro (Figure 1, *D*), whereas monomers of DiR in cores of PEG-*b*-PCL micelles at 1:400 ratio are quickly released over the first few hours. Thus, it was expected that monomeric DiR in PEG-*b*-PCL micelles would be highly fluorescent after injection and during release from polymeric micelles in vivo. In contrast, it was expected that aggregated DiR in PEG-*b*-PCL micelles would have a low fluorescence signal

after injection and that the optical signal would increase over time due to the release of DiR, which results in the loss of H-aggregates in PEG-*b*-PCL micelles and released monomeric DiR that is highly fluorescent.

Real time in vivo fluorescence images of DiR injected in either an aggregated state (1:40) or monomeric state (1:400) support these two mechanisms of NIR fluorescence imaging (Figures 2, *A* and 2, *B*). At a 1:40 ratio, the whole-body fluorescence signal from DiR was low and gradually emerged, especially near vascular tissue near the heart region and noticeably at the LS180 human colon carcinoma solid tumor after 4 hours. At a 1:400 ratio, the whole-body fluorescence signal from DiR was high even after 10 minutes and gradually lost intensity. However, the tumor in the flank region could be readily discerned after 4 hours and quite apparent after 9–24 hours after an increase in tumor signal and loss in background signal. Horizontal radiant efficiency maps going from the left flank to the tumor also showed that the NIR signal from DiR in an aggregated state was low in the left flank and the tumor, and over time the fluorescence signal built up at the tumor. At a 1:400 ratio, the fluorescence signal from DiR was strongest in the tumor and left flank after 10 minutes and selectivity for the tumor is gained over time, especially after 9 hours. Although the kinetics of in vivo fluorescence imaging of DiR depended on its aggregation state in PEG-*b*-PCL micelles, the whole-body optical imaging of tumors was quite similar in terms of selectivity, as shown in Figures 2, *E* and 2, *F*. The tumor to muscle ratio was about 2 after 9 hours at a 1:40 ratio and about 1.7 at a ratio of 1:400 at several time points. The tumor-to-muscle ratio indicates a measure of selectivity of an optical imaging agent comparing tumor accumulation to nontarget tissue (muscle). A tumor-to-muscle ratio greater than 1 suggests that the agent has distributed selectively to the tumor.[31] The Prosense 680 (Visen Medical, Woburn, Massachusetts), a commercially available NIR probe in preclinical development, has shown a tumor-to-muscle ratio of about 2.3 in vivo.[32] Therefore, DiR-incorporated PEG-*b*-PCL micelles gave equal or better tumor delineation. The tumor selectivity of DiR evidenced by optical imaging probably reflects the EPR effect, enabled by PEG-*b*-PCL micelles. However, pharmacokinetic experiments on DiR and PEG-*b*-PCL micelles are required to prove this hypothesis fully.

Surgical resection of various tissues at 96 hours after the injection of DiR-loaded PEG-*b*-PCL micelles, followed by optical imaging of DiR, confirmed the selectivity of the dye for tumor tissue regardless of the aggregation state of DiR in loaded PEG-*b*-PCL micelles (Figures 3, *A* and 3, *B*). It is noted that the average radiant efficiency of DiR is very high at the solid tumors, approximately 6.0×10^{10} p s^{-1} cm^{-2} sr^{-1}/[μW cm^{-2}], reflecting the selective tumor accumulation of DiR-loaded PEG-*b*-PCL micelles, high quantum yield, and dye stability even after 96 hours in vivo. In the excised organs, DiR had a remarkably high tumor-to-muscle ratio of 30-43.[31] In this experiment, optical imaging is done without the interference of overlying tissue, e.g., skin and blood vessels, and it more closely resembles intraoperative procedures in surgical oncology, as opposed to whole-body optical imaging that might have greater diagnostic value.

Surgical incision of mice followed by optical imaging of DiR revealed the clear delineation of tumor tissues (Figure 4, *A*). After the removal of skin overlying the tumor region and tumor resection, it was apparent under white light that tumor resection was complete (Figure 4, *B*). However, NIR optical imaging by DiR clearly provided evidence of remaining tumor margins (Figure 4, *C*). These in vivo results suggest that DiR-loaded PEG-*b*-PCL micelles can provide intraoperative guidance for the surgical removal of solid tumors. One limitation of this work is the use of a subcutaneous xenograft model rather than an orthotopic xenograft model that undergoes metastases. Future work will focus on the evaluation of DiR-loaded PEG-*b*-PCL micelles in an orthotopic xenograft model that will allow tests on the optical imaging of metastases, feasibility of their surgical removal, survival and a better delineation of the importance of DiR aggregation state on optical imaging.

Appendix A. Supplementary data

Supplementary materials related to this article can be found online at doi:10.1016/j.nano.2011.06.009.

References

1. Frangioni JV. In vivo near-infrared fluorescence imaging. Curr Opin Chem Biol 2003;7:626-34.
2. Yang Z, Zheng S, Harrison WJ, Harder J, Wen X, Gelovani JG, et al. Long-circulating near-infrared fluorescence core-cross-linked polymeric micelles: Synthesis, characterization, and dual nuclear/optical imaging. Biomacromolecules 2007;8:3422-8.
3. Leblond F, Davis SC, Valdes PA, Pogue BW. Pre-clinical whole-body fluorescence imaging: Review of instruments, methods and applications. J Photochem Photobiol B 2010;98:77-94.
4. Kumar R, Ohulchanskyy TY, Roy I, Gupta SK, Borek C, Thompson ME, et al. Near-infrared phosphorescent polymeric nanomicelles: Efficient optical probes for tumor imaging and detection. ACS Appl Mater Interfaces 2009;1:1474-81.
5. Altinoglu EI, Russin TJ, Kaiser JM, Barth BM, Eklund PC, Kester M, et al. Near-infrared emitting fluorophore-doped calcium phosphate nanoparticles for in vivo imaging of human breast cancer. ACS Nano 2008;2:2075-84.
6. Jiang S, Gnanasammandhan MK, Zhang Y. Optical imaging-guided cancer therapy with fluorescent nanoparticles. J R Soc Interface 2010;7:3-18.
7. Matsumura Y, Kataoka K. Preclinical and clinical studies of anticancer agent-incorporating polymer micelles. Cancer Sci 2009;100:572-9.
8. Soltesz EG, Kim S, Laurence RG, DeGrand AM, Parungo CP, Dor DM, et al. Intraoperative sentinel lymph node mapping of the lung using near-infrared fluorescent quantum dots. Ann Thorac Surg 2005;79:269-77.
9. Park K, Lee S, Kang E, Kim K, Choi K, Kwon IC. New generation of multifunctional nanoparticles for cancer imaging and therapy. Adv Funct Mater 2009;19:1553-66.
10. Luo L, Tam J, Maysinger D, Eisenberg A. Cellular internalization of poly(ethylene oxide)-b-poly(epsilon-caprolactone) diblock copolymer micelles. Bioconjug Chem 2002;13:1259-65.
11. Kwon G, Suwa S, Yokoyama M, Okano T, Sakurai Y, Kataoka K. Enhanced tumor accumulation and prolonged circulation times of micelle-forming poly (ethylene oxide-aspartate) block copolymer-adriamycin conjugates. J Control Release 1994;29:17-23.
12. Maeda H. Tumor-selective delivery of macromolecular drugs via the EPR effect. Background and future prospects Bioconjug Chem 2010;21:797-802.

13. Keramidas M, Josserand V, Righini CA, Wenk C, Faure C, Coll JL. Intraoperative near-infrared image-guided surgery for peritoneal carcinomatosis in a preclinical experimental model. Br J Surg 2010;97: 737-43.
14. Nguyen QT, Olson ES, Aguilera TA, Jiang T, Scadeng M, Ellies LG, et al. Surgery with molecular fluorescence imaging using activatable cell-penetrating peptides decreases residual cancer and improves survival. Proc Natl Acad Sci USA 2010;107:4317-22.
15. Trotter MJ, Chaplin DJ, Olive PL. Use of a carbocyanine dye as a marker of functional vasculature in murine tumours. Br J Cancer 1989;59:706-9.
16. Texier I, Goutayer M, Da Silva A, Guyon L, Djaker N, Josserand V, et al. Cyanine-loaded lipid nanoparticles for improved in vivo fluorescence imaging. J Biomed Opt 2009;14:054005-2.
17. Liu J, Zeng F, Allen C. In vivo fate of unimers and micelles of a poly(ethylene glycol)-block-poly(caprolactone) copolymer in mice following intravenous administration. Eur J Pharm Biopharm 2007;65:309-19.
18. Forrest ML, Zhao A, Won CY, Malick AW, Kwon GS. Lipophilic prodrugs of Hsp90 inhibitor geldanamycin for nanoencapsulation in poly(ethylene glycol)-b-poly(epsilon-caprolactone) micelles. J Control Release 2006;116:139-49.
19. Forrest ML, Won CY, Malick AW, Kwon GS. In vitro release of the mTOR inhibitor rapamycin from poly(ethylene glycol)-b-poly(epsilon-caprolactone) micelles. J Control Release 2006;110: 370-7.
20. Forrest ML, Yanez JA, Remsberg CM, Ohgami Y, Kwon GS, Davies NM. Paclitaxel prodrugs with sustained release and high solubility in poly(ethylene glycol)-b-poly(epsilon-caprolactone) micelle nanocarriers: pharmacokinetic disposition, tolerability, and cytotoxicity. Pharm Res 2008;25:194-206.
21. Tian Y, Wu WC, Chen CY, Jang SH, Zhang M, Strovas T, et al. Utilization of micelles formed from poly(ethylene glycol)-block-poly(epsilon-caprolactone) block copolymers as nanocarriers to enable hydrophobic red two-photon absorbing emitters for cells imaging. J Biomed Mater Res A 2010;93:1068-79.
22. Kumar V, Prud'homme RK. Thermodynamic limits on drug loading in nanoparticle cores. J Pharm Sci 2008;97:4904-14.
23. Mikhail AS, Allen C. Block copolymer micelles for delivery of cancer therapy: Transport at the whole body, tissue and cellular levels. J Control Release 2009 Sep 15;138:214-23.
24. Maiti NC, Mazumdar S, Periasamy N. J- and H-aggregates of porphyrin-surfactant complexes: time-resolved fluorescence and other spectroscopic studies. J Phys Chem 1998;102:1528-38.
25. Khairutdinov RF, Serpone N. Photophysics of cyanine dyes: subnanosecond relaxation dynamics in monomers, dimers, and H- and J-aggregates in solution. J Phys Chem 1997;101:2602-10.
26. Tummino PJ, Gafni A. Determination of the aggregation number of detergent micelles using steady-state fluorescence quenching. Biophys J 1993;64:1580-7.
27. Lee S, Ryu JH, Park K, Lee A, Lee S, Youn I, et al. Polymeric nanoparticle-based activatable near-infrared nanosensor for protease determination in vivo. Nano Letts 2009;9:4412-6.
28. Zeisser-Labouebe M, Mattiuzzo M, Lange N, Gurny R, Delie F. Quenching-induced deactivation of photosensitizer by nanoencapsulation to improve phototherapy of cancer. J Drug Target 2009;17:619-26.
29. Xinzhan P, Huaxian C, Daniel RD, William V, Amy SD. A non-fluorescent, broad range quencher dye for FRET assays. Anal Biochem 2009;338:220-8.
30. Behera GB, Behera PK, Mishra BK. J. Cyanine dyes: self aggregation and behaviour in surfactants. J Surface Sci Technol 2007;23:2-31.
31. Miao Z, Ren G, Liu H, Jiang L, Cheng Z. Cy5.5-labeled affibody molecule for near-infrared fluorescent optical imaging of epidermal growth factor receptor positive tumors. J Biomed Opt 2010;15:036007.
32. Olson ES, Jiang T, Aguilera TA, Nguyen QT, Ellies LG, Scadeng M, et al. Activatable cell penetrating peptides linked to nanoparticles as dual probes for in vivo fluorescence and MR imaging of proteases. Proc Natl Acad Sci USA 2010;107:4311-6.